CUSTOMIZED WO_3 NANOPLATELETS AS VISIBLE-LIGHT PHOTOELECTROCATALYST FOR THE DEGRADATION OF A RECALCITRANT MODEL ORGANIC COMPOUND (METHYL ORANGE)

Fernández-Domene, R.M.; Sánchez-Tovar, R.; Lucas-Granados, B. ; García-Zamora, C.S.; García-Antón, J.

Ingeniería Electroquímica y Corrosión (IEC). Departamento de Ingeniería Química y Nuclear. ETSI Industriales. Universitat Politècnica de València. Camino de Vera s/n, 46022 Valencia, Spain. Tel. 34-96-387 76 32, Fax. 34-96-387 76 39,

e-mail: *jgarciaa@iqn.upv.es (J. García-Antón).*

WO_3 nanoplatelets have been synthesized by electrochemical anodization in acidic electrolytes containing two different complexing agents: fluorides and hydrogen peroxide. The influence of the morphology and size of these nanoplatelets on their photoelectrocatalytic performance has been studied following the degradation of a model organic recalcitrant compound, such as methyl orange (MO). The effect of several supporting electrolytes on this photodegradation process has also been checked. The best MO decoloration was observed for nanoplatelets fabricated in the presence of low H_2O_2 concentrations, whose distribution and small size made them expose a very high surface area to the problem solution. With this nanostructure, decoloration efficiencies of ca. 100% were obtained after just 60 min. This result is considerably better than others reported in similar works, indicating the excellent behavior of these WO_3 nanoplatelets as photoelectrocatalysts.

KEYWORDS: WO_3 nanostructures, photoelectrocatalysis, methyl orange, complexing agents, anodization.

1. Introduction

Water is one of the most essential resources on Earth, being crucial to all living cells and hence being responsible for life on the planet. With the human body consisting of 75 % of water, this substance is indispensable for human health and well-being, as well as for environmental preservation. Water covers more than 70% of the earth's surface, but 97% of it is salty and only 3% is fresh. Of this fresh water, more than two thirds are retained in the form of ice in the continental ice caps and glaciers, ground water accounts for about 30% and only 0.26% of global freshwater reserves are found in lakes and rivers [1]. In spite of being essential for life, water is also the world's most threatened essential resource, and the growing scarcity of freshwater resources is among the main challenges of the 21st century. One factor that decisively contributes to this freshwater shortage is the increasing pollution of water bodies due to the action of human beings.

Among the most problematic pollutants found in aquatic ecosystems are recalcitrant organic compounds, such as pesticides, drugs or dyes. These compounds and their metabolites are normally non-biodegradable, so conventional biological oxidation treatments are not useful [2]. Several advanced oxidation processes have been proposed as alternative to remove these compounds. Photoelectrocatalytic methods, which combine electrochemical and photo-catalysis technologies, have recently raised great interest due to their high efficiencies and low cost in removing persistent pollutants from aqueous electrolytes [2-18].

Photoelectrochemistry deals with processes taking place at a semiconductor electrode under illumination, where electron-hole pairs are photogenerated and separated due to the action of an electric field inside the semiconductor. In *n*-type semiconductors (photoanodes), electrons move towards the back contact and, through an external circuit, to the cathode, while holes move towards the semiconductor/electrolyte interface, where they can oxidize the species present in the solution.

Nanostructured semiconductor metal oxides, such as TiO_2 or WO_3, are increasingly employed as photoanodes in photoelectrocatalytic processes, due to their higher surface areas in contact with the electrolyte, which increases the number of active sites and improves charge transfer processes and light absorption. Tungsten trioxide is a material with a band-gap value of ca. 2.6 eV that can therefore absorb light within the visible region of the solar spectrum (up to ca. 480 nm) [19-21]. Moreover, holes in the valence band of WO_3 have a potential of 2.97 V_{HNE} at pH 0 [22], which is enough to oxidize water and to form oxidative species.

Anodization is one of the simplest methods used to synthesize nanostructured WO_3 photoanodes. Besides, a controlled change in the different anodization conditions (applied potential, temperature, anodization time, electrolyte composition, etc.) permits a wide range of morphologies and dimensions, and these nanostructures are directly bound to the metallic back contact, improving significantly the efficiency of electron collection. Furthermore, since the nanostructured photocatalyst is firmly attached to the substrate, its separation from the solution upon finishing the water treatment process is not necessary, thus avoiding the loss of material. In this study, different tungsten trioxide (WO_3) nanostructures synthesized by anodization under hydrodynamic

conditions have been used to eliminate methyl orange (MO), a persistent organic pollutant used in this work as a model organic molecule. The objective of the work is to analyze the influence of the morphology and size of WO_3 nanostructures, as well as some experimental conditions, such as the nature of the electrolyte or the wavelength of the incident light, on the MO removal efficiency.

2. Experimental procedure

2.1 Fabrication of WO_3 nanostructures by anodization

The different WO_3 nanostructures used in this work were synthesized by electrochemical anodization. Tungsten rods (8 mm in diameter) exposing 0.5 cm^2 to the electrolyte were used as working electrodes, while a platinum mesh was used as the counter electrode. Tungsten rods were covered with a Teflon coating to prevent the rest of the surface from contacting the electrolyte. The platinum mesh (cathode) was placed in the cell so as it surrounded the working electrode (anode), and the distance between them was constant (1 cm, concentrically). In a previous step, the tungsten surface was wet abraded with 200, 500 and 4000 grit SiC papers, rinsed with distilled water, dried with pressured air, degreased by sonication in ethanol for 2 minutes, rinsed and dried again. Anodization was carried out under controlled hydrodynamic conditions by using a Rotating Disk Electrode (at 375 rpm [23, 24]), imposing a constant cell potential of 20 V and a temperature of 50º C for 4 hours.

In a previous work [24] it has been observed that the morphology and dimensions of WO_3 nanostructures can be controlled by using small amounts of different complexing

agents, such as fluoride anions or hydrogen peroxide. Hence, in order to obtain nanostructures with different morphologies, several anodization electrolytes were used: (1) 1.5 M H_2SO_4; (2) 1.5 M H_2SO_4 + 0.1 M NaF; (3) 1.5 M H_2SO_4 + 0.05 M H_2O_2.

The as-anodized samples were then annealed in a cylindrical oven at 400º C for 4 hours in an air atmosphere to obtain a crystalline phase. The crystalline microstructure of the WO_3 nanostructures was examined by means of a Raman Confocal Laser microscopy, using a 632 nm neon laser with 420 μW. The morphology of the obtained nanostructures was observed by a Field Emission Scanning Electron Microscopy (FESEM).

2.2 Photoelectrocatalytic degradation of methyl orange

Photoelectrocatalytic degradation of MO was conducted at room temperature in a quartz glass three-electrode photoelectrochemical cell. The WO_3 nanostructures (exposing an area to the solution of 0.5 cm^2) were used as working electrodes, an Ag/AgCl (3M KCl) electrode acted as reference electrode and a platinum tip was used as counter electrode. A bias potential of 1V was applied during the photoelectrocatalytic degradation tests by using an Autolab PGSTAT302N potentiostat. Current densities were measured during the tests and photocurrent densities (i_{ph}) were determined by subtracting dark-current density values from total current densities.

The initial MO concentration was 50 μM and the reaction volume was always 12 cm^3. The influence of supporting electrolytes with different acidity was studied by adding 0.1 M Na_2SO_4 or 0.1 M H_2SO_4. The solution was agitated during the whole test by using a

magnetic stirrer to obtain homogeneous conditions inside the cell. The samples were perpendicularly irradiated with a 1000 W Xe light source, with different values of wavelength (360 nm and 420 nm), and the distance between the samples and the lamp was a constant value of 5 cm (the light power density measured at that distance was 40 mW cm^{-2} at 360 nm and 100 mW cm^{-2} at 420 nm). Prior to the irradiation, samples were immersed in the MO solution for 30 minutes at their open circuit potential to attain initial equilibrium conditions.

After every 20 minutes of reaction under irradiation, 3 mL of the solution were withdrawn from the glass cell to monitor the photoelectrocatalytic degradation process by means of UV-visible spectrophotometry, measuring the absorbance of MO in a wide range of wavelengths (from 190 nm to 800 nm). After the measuring, the aliquot was returned to the reactor. The decoloration efficiency was determined according to the following equation:

$$\eta = \frac{C_0 - C}{C_0} \times 100 \quad \textbf{(1)}$$

where C_0 is the maximum absorbance of the initial MO solution and C is the maximum absorbance of the MO solution at a certain reaction time.

3. Results and discussion

3.1. Morphological and compositional characterization of WO_3 nanostructures

The morphological characterization of the different nanostructures was performed through FESEM. The images of these nanostructures are depicted in **Figure 1**. For the sample anodized in the 1.5 M H_2SO_4 electrolyte, disordered nanoplatelets could be observed throughout the surface (**Figure 1a**). Some of these nanoplatelets grew in a perpendicular way, whereas others (smaller) grew almost parallel to the surface. This morphology has been typically obtained when anodizing tungsten in acidic environments under moderate or high temperature [25-27]. When synthesized in the presence of complexing agents (fluoride anions and hydrogen peroxide), nanoplatelets were also obtained, but their size and distribution was very different. In the 0.1 M F^- solution, nanoplatelets grew in spherical fashion, ordered in tree-like structures (**Figure 1b**). The morphology of this nanostructure resulted in a surface area higher than in the absence of fluoride anions [23, 27]. On the other hand, in the presence of 0.05 M H_2O_2, the size of the obtained nanoplatelets was significantly lower than in the other two cases (**Figure 1c**), and they aggregated forming very thin layers [24]. The reduced dimensions of this nanostructure may also imply an increase in the surface area with respect to other WO_3 nanoplatelets.

Figure 1d shows the Raman spectra of the three different nanostructures after the thermal process. It can be observed that there are no differences between them, indicating that the composition and crystalline phase of the different nanoplatelets are the same. A series of characteristic peaks related to the monoclinic and/or orthorhombic crystalline phases of WO_3 can be clearly observed in all cases. At low Raman displacements (between ~190 and ~330 cm^{-1}), three peaks corresponding with bending vibration of (O─W─O) bonds and lattice modes of crystalline WO_3 can be discerned. The highest peaks, located at ~710 cm^{-1} and ~810 cm^{-1} are characteristic of the

symmetric stretching vibration of (O─W─O) bonds. These results indicate that annealed nanostructures consisted of dehydrated crystalline WO_3 [26, 28-30]

3.2. Photoelectrocatalytic degradation of MO

Figure 2a shows the time evolution of the ratio between the MO absorbance (or concentration) at a given time and the initial MO absorbance (or concentration), C/C_0, for the three different WO_3 nanostructures. The used solution, in this case, consisted only of 50 μM MO, that is, without adding any supporting electrolyte. The decoloration efficiency under those experimental conditions is shown in **Figure 2b**. It can be observed that low values of C/C_0 and high values of decoloration efficiency (70-80%) were achieved for the three WO_3 nanostructures after 180 minutes of photoelectrochemical reaction. The concentration of MO decreased slightly faster for the nanostructure synthesized in the 1.5 M H_2SO_4 electrolyte (without complexing agent).

The photocurrent density mean values (i_{ph}) recorded during the photoelectrocatalytic tests (without supporting electrolyte) are shown in **Figure 3**. Photocurrent densities were higher for the sample anodized in the 1.5 M H_2SO_4 electrolyte than for the rest of the samples. This means that, upon illumination in the MO solution without supporting electrolyte, the highest concentration of photogenerated electron/hole (e^-/h^+) pairs was obtained for the nanoplatelets synthesized in the 1.5 M H_2SO_2 electrolyte. The lower i_{ph} values for the other two nanostructures could be explained by taking into account the low solution conductivity and their morphology and size, as it will be explained below. Anyway, the higher amount of e^-/h^+ pairs is directly related to the photocurrent density

values. On the other hand, as observed above, the nanostructure formed in the 1.5 M H_2SO_4 electrolyte (disordered nanoplatelets) produced the highest decoloration efficiencies when working without any supporting electrolyte (**Figure 2**). However, the differences in photoelectrocatalytic behavior between the three nanostructures were not so marked as their i_{ph} values. Indeed, although the nanoplatelets synthesized in the ligand-free electrolyte (1.5 M H_2SO_4) generated a higher concentration of h^+, it can be assumed that a substantial part of these holes were not used in the photodegradation process. This could be related to a certain difficulty for MO molecules to adsorb on the nanoplatelets surface, which would partially obstruct their interaction with surface holes or oxygen radicals (such as surface hydroxyl radicals). Hence, in the present case, there is not a so clear relationship between i_{ph} values and photoelectrodegradation efficiency.

To find out whether the addition of a supporting electrolyte can improve the photoelectrocatalytic response of the studied nanostructures, 0.1 M Na_2SO_4 were added to the MO solution. Ionic conductivity is a decisive parameter to assure an efficient performance of nanostructured photoelectrodes, especially of those with high thicknesses or porous morphology. These nanostructures, whose morphology may limit its performance, must be completely permeated by the electrolyte to present a good photoelectrochemical behavior, and this can be achieved by using electrolytes with high conductivities [31]. The decoloration profiles presented in **Figure 4** for the three WO_3 nanostructures show the effect of adding 0.1 M Na_2SO_4 to the 50 μM MO solution. Despite of the type of nanostructure employed, the lowest degradation rates were always obtained in the sulphate electrolyte. The same can be said for the decoloration efficiency (**Figure 5**), i.e., in the presence of Na_2SO_4, the photoelectrochemical performance of the WO_3 nanostructures significantly worsened. To see whether this

reduction in photoelectrocatalytic performance was related to a decrease in the generation of reactive holes (h^+), photocurrent density transients were recorded throughout the process and their mean values are shown in **Figure 6**. It can be clearly seen that photocurrent density values considerably decreased in the solution containing SO_4^{2-} anions, regardless of the type of nanoplatelets. Moreover, in general, i_{ph} tended to decrease with time in the sulphate-containing solution.

According to several authors [4, 9], anions such as SO_4^{2-} can adsorb on the nanostructures surface and react with photogenerated holes, thus competing with MO molecules for adsorption sites. This fact might explain the lower rates of decoloration obtained in the presence of Na_2SO_4, making the addition of supporting electrolyte be a negative factor for the photocatalytic performance of the WO_3 nanostructures. However, another important parameter must be taken into account when discussing the influence of Na_2SO_4 added to the MO solution on the photoelectrochemical response of the different samples: the electrolyte pH. The pH of the MO solution without supporting electrolyte was 5.1, while the pH of the MO-sulphate electrolyte was 5.8, almost a unit higher.

In this work, WO_3 nanostructures were formed by electrochemical anodization following a dissolution/precipitation mechanism. According to this mechanism, tungsten soluble complex species were formed by the reaction between H^+, F^- and/or H_2O_2, on the one hand, and the substrate (W and WO_3), on the other hand. In highly acidic environments (pH < 1), these soluble species formed poly-condensed molecules that eventually (upon reaching supersaturation conditions) precipitated on the tungsten electrode surface as tungstic acids ($WO_3 \cdot H_2O$ and $WO_3 \cdot 2H_2O$) in the form of

nanoplatelets. The size and morphology of these nanostructures was directly related to the absence/presence of complexing agents in the anodization solution (F^- or H_2O_2) and to their concentration [24]. Since an acidic environment is crucial for the poly-condensation of tungsten complex species and, hence, for the formation of hydrated WO_3 nanoplatelets according to the aforementioned dissolution/precipitation mechanism, it is logical to assume that the stability of these nanostructures and their photoelectrochemical performance strongly depends on the solution pH. Indeed, WO_3 and its hydrated forms are stable in acidic media and start dissolving at neutral, and especially alkaline, pH values [32]. In a recent work [23] it was demonstrated that the photoelectrochemical performance of WO_3 nanoplatelets improved in acidic electrolytes.

In accordance with the explanations given above, H_2SO_4 was also used as a supporting electrolyte by adding 0.1 M H_2SO_4 to the MO solution. **Figure 7** compares the decoloration profiles for the three studied WO_3 nanostructures in the MO solution without supporting electrolyte and in the acidic MO solution. The corresponding percentage of decoloration efficiency is shown in **Figure 8**. It can be observed that the addition of 0.1 M H_2SO_4 to the 50 μM MO solution greatly enhanced the photoelectrocatalytic ability of the three types of WO_3 nanoplatelets. Nevertheless, this increase was especially outstanding for the nanostructure synthesized in the 0.05 M H_2O_2 solution, where the total decoloration of the solution was achieved after only 1 hour of treatment.

The excellent behavior (in acidic media) of the nanoplatelets formed in the presence of peroxides can be related to their morphology and size. The dimensions of these

nanoplatelets were very low, which could lead to electroactive surface areas higher than for the rest nanostructures, hence increasing the formation of photogenerated electron-hole pairs. Besides, the arrangement of these small nanoplatelets forming very thin and compact layers could improve the separation of photogenerated charges [24]. Photocurrent density transients recorded in the solution with 0.1 M H_2SO_4 for the three types of WO_3 nanoplatelets (**Figure 9**) indicate that the sample anodized in the 0.05 M H_2O_2 solution provided the highest photocurrent density values, significantly higher than for the rest of the samples. This result is consistent with the suggestion made above, that is, that the sample synthesized in the presence of peroxides had higher electroactive surfaces areas due to the extremely small size of the nanoplatelets, leading to higher formation of e^-/h^+ pairs and improving charge transfer processes.

On the other hand, photocurrent densities for the other two samples were similar, which is also consistent with their comparable decoloration profiles and efficiencies in the acidic MO solution (**Figures 7** and **8**). Observing the FESEM images of the different nanoplatelets (**Figure 1**), it is evident that the nanostructure synthesized in the 0.1 M NaF solution presented a considerably higher surface area than the one fabricated in the ligand-free solution (1.5 M H_2SO_4), due to its tree-like morphology and notably higher thickness. In fact, in different works [24, 27], it was demonstrated that the photoelectrochemical performance of WO_3 nanoplatelet globular clusters under simulated sunlight was better than that of simple nanoplatelets. However, in the present case, the photocatalytic behavior of both nanostructures can be regarded as similar in the acidic MO solution. This can be related to the fact that, in the presence of F^- anions, not all the electrode surface was covered with nanoplatelets. As explained in another paper [23], at a rotation velocity of 375 rpm and in the 1.5 M H_2SO_4 + 0.1 M NaF

anodization solution, the electrode geometric area covered with nanostructures was of 66% (approximately 0.33 cm^2, instead of 0.5 cm^2 of total surface). Hence, the photoresponse of this sample had two contributions, i.e., the area covered by nanoplatelet globular clusters (0.33 cm^2) and the area uncovered by nanoplatelets and covered by a thin and compact WO_3 layer, much less active to irradiated light (0.17 cm^2). In the other two samples, nanostructures covered the whole surface. The above explanation leads to the conclusion that nanoplatelets formed in the F^--containing solution (growing in a tree-like fashion) are more active than conventional nanoplatelets, since both samples presented similar photoelectrocatalytic behavior but the geometric area of the former is a 34% lower than that of the latter.

In order to investigate the capacity of the high-performance small nanoplatelets fabricated in the 0.05 M H_2O_2 electrolyte to absorb visible light and to operate under that illumination, degradation tests were also carried out at a wavelength of 420 nm. The decoloration profile and decoloration efficiency obtained for this nanostructure in an acidic environment at 420 nm are shown in **Figure 10**. It can be observed that the MO molecules were completely degraded after 140 minutes of visible light illumination. These results are significantly better than visible-light photoelectrocatalytic MO degradation results reported by other authors for two reasons. First, because in the present case a 100% of decoloration efficiency under visible light was reached after 140 minutes, while in other works, longer times were needed for that purpose (from 180 minutes [9] to 360 minutes [33], even when working with doped WO_3 photocatalysts [12]). Second, because in all those works, the photoelectrodes geometric area exposed to the electrolyte and to illumination was much higher (from 12 cm^2 [9] to 64 cm^2 [12, 33]), while in this work the exposed area was only 0.5 cm^2.

Taking into account that in this study the total reaction volume was 12 cm^3, the ratio between the electrode geometric area and the reaction volume was 0.042 cm^{-1}, whereas in the other works, this ratio notably increased to 0.256 cm^{-1} [12] and to 0.6 cm^{-1} [9].

4. Conclusions

Different WO_3 nanoplatelets were obtained by anodization of tungsten, depending on the used electrolyte. In the 0.05 M H_2O_2 electrolyte, very small nanoplatelets or nanosheets arranged in very thin layers were fabricated.

In all cases, the addition of 0.1 M Na_2SO_4 as supporting electrolyte to the MO solution negatively affected the decoloration efficiency of the nanostructures. This result is directly related to the nearly neutral pH of the sulphate solution. Hence, a low pH was found necessary to enhance the photoelectrochemical performance of these nanostructures.

With the addition of 0.1 M H_2SO_4 to the MO solution, the decoloration efficiency substantially increased, especially for nanoplatelets formed in the 0.05 M H_2O_2 solution. The especially good behavior of that nanostructure can be attributed to a higher surface area due to the lower nanoplatelet/nanosheet dimensions, as well as to enhanced electron transport towards the metallic back contact.

Under blue light (420 nm), the decoloration efficiency of this nanostructure was very good. Results obtained in this work are significantly better than visible-light photoelectrocatalytic MO degradation results reported by other authors.

Acknowledgements

Authors thank for the financial support to the Ministerio de Economía y Competitividad (Project Code: CTQ2016-79203-R), for its help in the Laser Raman Microscope acquisition (UPOV08-3E-012), and for the co-finance by the European Social Fund.

References

[1] Igor A.Shiklomanov, World fresh water resources, in: Peter H.Gleick (ed.), Water Crisis: A guide to world's fresh water resources, Oxford University Press, New York, 1993, 13-24.

[2] R. Daghrir, P. Drogui, D. Robert. Photoelectrocatalytic technologies for environmental applications, J. Photoch. Photobio. A 238 (2012) 41-52.

[3] S. Garcia-Segura, E. Brillas. Applied photoelectrocatalysis on the degradation of organic pollutants in wastewaters, J. Photoch. Photobio. C 31 (2017) 1-35.

[4] J. Luo, M. Hepel. Photoelectrochemical degradation of naphthol blue black diazo dye on WO_3 film electrode, Electrochim. Acta 46 (2001) 2913-2922.

[5] X. F. Cheng, W. H. Leng, D. P. Liu, J. Q. Zhang, C. N. Cao. Enhanced photoelectrocatalytic performance of Zn-doped WO_3 photocatalysts for nitrite ions degradation under visible light, Chemosphere 68 (2007) 1976-1984.

[6] D. Monllor-Satoca, L. Borja, A. Rodes, R. Gómez, P. Salvador. Photoelectrochemical Behavior of Nanostructured WO_3 Thin-Film Electrodes: The Oxidation of Formic Acid, ChemPhysChem 7 (2006) 2540-2551.

[7] X. He, Y. Cai, H. Zhang, C. Liang. Photocatalytic degradation of organic pollutants with Ag decorated free-standing TiO_2 nanotube arrays and interface electrochemical response, J. Mater. Chem. 21 (2011) 475-480.

[8] R. Mohammadpour, A. Irajizad, N. Taghavinia, M. Rahman, M. M. Ahadian. Electrochemically Assisted Photocatalytic Oxidation of Methanol on TiO_2 Nanotube Arrays, J. Mater. Sci. Technol. 26 (2010) 535-541.

[9] Q. Zheng, C. Lee. Visible light photoelectrocatalytic degradation of methyl orange using anodized nanoporous WO_3, Electrochim. Acta 115 (2014) 140-145.

[10] C. J. Lin, S. J. Liao, L. C. Kao, S. Y. H. Liou. Photoelectrocatalytic activity of a hydrothermally grown branched Zno nanorod-array electrode for paracetamol degradation, J. Hazard. Mater. 291 (2015) 9-17.

[11] G. Longobucco, L. Pasti, A. Molinari, N. Marchetti, S. Caramori, V. Cristino, R. Boaretto, C. A. Bignozzi. Photoelectrochemical mineralization of emerging contaminants at porous WO_3 interfaces, Appl. Catal. B: Environ. 204 (2017) 273-282.

[12] S. V. Mohite, V. V. Ganbavle, K. Y. Rajpure. Photoelectrocatalytic activity of immobilized Yb doped WO_3 photocatalyst for degradation of methyl orange dye, J. Energy Chem. 26 (2017) 440-447.

[13] L. Liu, R. Li, Y. Liu, J. Zhang. Simultaneous degradation of ofloxacin and recovery of Cu(II) by photoelectrocatalysis with highly ordered TiO_2 nanotubes, J. Hazard. Mater. 308 (2016) 264-275.

[14] I. Tantis, L. Bousiakou, Z. Frontistis, D. Mantzavinos, I. Konstantinou, M. Antonopoulou, G. A. Karikas, P. Lianos. Photocatalytic and photoelectrocatalytic degradation of the drug omeprazole on nanocrystalline titania films in alkaline media: Effect of applied electrical bias on degradation and transformation products, J. Hazard. Mater. 294 (2015) 57-63.

[15] Y.M. Hunge, Sunlight assisted photoelectrocatalytic degradation of benzoic acid using stratified WO_3/TiO_2 thin films, Ceram. Int. 43 (2017) 10089-10096.

[16] Y.M. Hunge, M.A. Mahadik, A.V. Moholkar, C.H. Bhosale, Photoelectrocatalytic degradation of oxalic acid using WO_3 and stratified WO_3/TiO_2 photocatalysts under sunlight illumination, Ultrason. Sonochem. 35 (2017) 233-242.

[17] Y.M. Hunge, M.A. Mahadik, A.V. Moholkar, C.H. Bhosale, Photoelectrocatalytic degradation of phthalic acid using spray deposited stratified WO_3/ZnO thin films under sunlight illumination, Appl. Surf. Sci. 420 (2017) 764-772.

[18] Y.M. Hunge, M.A. Mahadik, V.L. Patil, A.R. Pawar, S.R. Gadakh, A.V. Moholkar, P.S. Patil, C.H. Bhosale, Visible light assisted photoelectrocatalytic degradation of sugarcane factory wastewater by sprayed CZTS thin films, J. Phys. Chem. Sol. 111 (2017) 176-181.

[19] H. Zheng, J. Z. Ou, M. S. Strano, R. B. Kaner, A. Mitchell, K. Kalantar-zadeh. Nanostructured Tungsten Oxide - Properties, Synthesis, and Applications, Adv. Funct. Mater. 21 (2011) 2175-2196.

[20] C. A. Bignozzi, S. Caramori, V. Cristino, R. Argazzi, L. Meda, A. Tacca. Nanostructured photoelectrodes based on WO_3: applications to photooxidation of aqueous electrolytes, Chem. Soc. Rev. 42 (2013) 2228-2246.

[21] A. Di Paola, E. García-López, G. Marcì, L. Palmisano. A survey of photocatalytic materials for environmental remediation, J. Hazard. Mater. 211-212 (2012) 3-29.

[22] L. Weinhardt, M. Blum, M. Bär, C. Heske, B. Cole, B. Marsen, E. L. Miller. Electronic Surface Level Positions of WO_3 Thin Films for Photoelectrochemical Hydrogen Production, J. Phys. Chem. C 112 (2008) 3078-3082.

[23] R. M. Fernández-Domene, R. Sánchez-Tovar, B. Lucas-Granados, J. García-Antón. Improvement in photocatalytic activity of stable WO_3 nanoplatelet globular clusters arranged in a tree-like fashion: Influence of rotation velocity during anodization, Appl. Catal. B Environ. 189 (2016) 266-282.

[24] R. M. Fernández-Domene, R. Sánchez-Tovar, B. Lucas-Granados, G. Roselló-Márquez, J. García-Antón. A simple method to fabricate high-performance nanostructured WO_3 photocatalysts with adjusted morphology in the presence of complexing agents, Mater. Design 116 (2017) 160-170.

[25] K. Kalantar-zadeh, A. Z. Sadek, H. Zheng, V. Bansal, S. K. Bhargava, W. Wlodarski, J. Zhu, L. Yu, Z. Hu. Nanostructured WO_3 films using high temperature anodization, Sensor. Actuat. B-Chem. 142 (2009) 230-235.

[26] A. Z. Sadek, H. Zheng, M. Breedon, V. Bansal, S. K. Bhargava, K. Latham, J. Zhu, L. Yu, Z. Hu, P. G. Spizzirri, W. Wlodarski, K. Kalantar-zadeh. High-Temperature Anodized WO_3 Nanoplatelet Films for Photosensitive Devices, Langmuir 25 (2009) 9545-9551.

[27] R. M. Fernández-Domene, R. Sánchez-Tovar, E. Segura-Sanchís, J. García-Antón. Novel Tree-Like WO_3 Nanoplatelets with Very High Surface Area Synthesized by Anodization Under Controlled Hydrodynamic Conditions, Chem. Eng. J. 286 (2015) 59-67.

[28] M. F. Daniel, B. Desbat, J. C. Lassegues, B. Gerand, M. Figlarz. Infrared and Raman study of WO_3 tungsten trioxides and WO_3, xH_2O tungsten trioxide tydrates, J. Solid State Chem. 67 (1987) 235-247.

[29] B. Pecquenard, H. Lecacheux, J. Livage, C. Julien. Orthorhombic WO_3 Formed via a Ti-Stabilized $WO_3 \cdot 13H_2O$ Phase, J. Solid State Chem. 135 (1998) 159-168.

[30] F. Amano, M. Tian, B. Ohtani, A. Chen. Photoelectrochemical properties of tungsten trioxide thin film electrodes prepared from facet-controlled rectangular platelets, J. Solid State Electrochem. 16 (2012) 1965-1973.

[31] R. Solarska, R. Jurczakowski, J. Augustynski. A highly stable, efficient visible-light driven water photoelectrolysis system using a nanocrystalline WO_3 photoanode and a methane sulfonic acid electrolyte, Nanoscale 4 (2012) 1553-1556.

[32] E. Lassner and W. D. Schubert, Tungsten. Properties, Chemistry, Technology of the Element, Alloys, and Chemical Compounds, Kluwer Academic / Plenum Publishers, New York, 1999.

[33] Y. M. Hunge, M. A. Mahadik, S. S. Kumbhar, V. S. Mohite, K. Y. Rajpure, N. G. Deshpande, A. V. Moholkar, C. H. Bhosale. Visible light catalysis of methyl orange using nanostructured WO_3 thin films, Ceram. Int. 42 (2016) 789-798.

Figures captions

Figure 1. FESEM images of the WO_3 nanostructures formed by anodization in (a) 1.5 M H_2SO_4, (b) 1.5 M H_2SO_4 + 0.1 M NaF and (c) 1.5 M H_2SO_4 + 0.05 M H_2O_2. (d) Raman spectra of the samples after the heat treatment at 400 ºC for 4h.

Figure 2. Decoloration profiles (a) and decoloration efficiency (b) for the three different WO_3 nanostructures (50 μM MO).

Figure 3. Photocurrent density mean values (i_{ph}) recorded during the photoelectrocatalytic tests (50 μM MO).

Figure 4. Decoloration profiles in 50 μM MO + 0.1 M Na_2SO_4 for the three different WO_3 nanostructures: (a) nanostructure anodized in 1.5 M H_2SO_4, (b) nanostructure anodized in 1.5 M H_2SO_4 + 0.1 M NaF and (c) nanostructure anodized in 1.5 M H_2SO_4 + 0.05 M H_2O_2.

Figure 5. Decoloration efficiency in 50 μM MO + 0.1 M Na_2SO_4 for the three different WO_3 nanostructures: (a) nanostructure anodized in 1.5 M H_2SO_4, (b) nanostructure anodized in 1.5 M H_2SO_4 + 0.1 M NaF and (c) nanostructure anodized in 1.5 M H_2SO_4 + 0.05 M H_2O_2.

Figure 6. Photocurrent density mean values in 50 μM MO + 0.1 M Na_2SO_4 for the three different WO_3 nanostructures: (a) nanostructure anodized in 1.5 M H_2SO_4, (b)

nanostructure anodized in 1.5 M H_2SO_4 + 0.1 M NaF and (c) nanostructure anodized in 1.5 M H_2SO_4 + 0.05 M H_2O_2.

Figure 7. Decoloration profiles in 50 μM MO + 0.1 M H_2SO_4 for the three different WO_3 nanostructures: (a) nanostructure anodized in 1.5 M H_2SO_4, (b) nanostructure anodized in 1.5 M H_2SO_4 + 0.1 M NaF and (c) nanostructure anodized in 1.5 M H_2SO_4 + 0.05 M H_2O_2.

Figure 8. Decoloration efficiency in 50 μM MO + 0.1 M H_2SO_4 for the three different WO_3 nanostructures: (a) nanostructure anodized in 1.5 M H_2SO_4, (b) nanostructure anodized in 1.5 M H_2SO_4 + 0.1 M NaF and (c) nanostructure anodized in 1.5 M H_2SO_4 + 0.05 M H_2O_2.

Figure 9. Photocurrent density mean values recorded during the photoelectrocatalytic tests in 50 μM MO + 0.1 M H_2SO_4 for the three WO_3 nanostructures.

Figure 10. Decoloration profile and decoloration efficiency in 50 μM MO + 0.1 M H_2SO_4 for the nanostructure anodized in 1.5 M H_2SO_4 + 0.05 M H_2O_2 under a 420 nm irradiation.

Figure 1

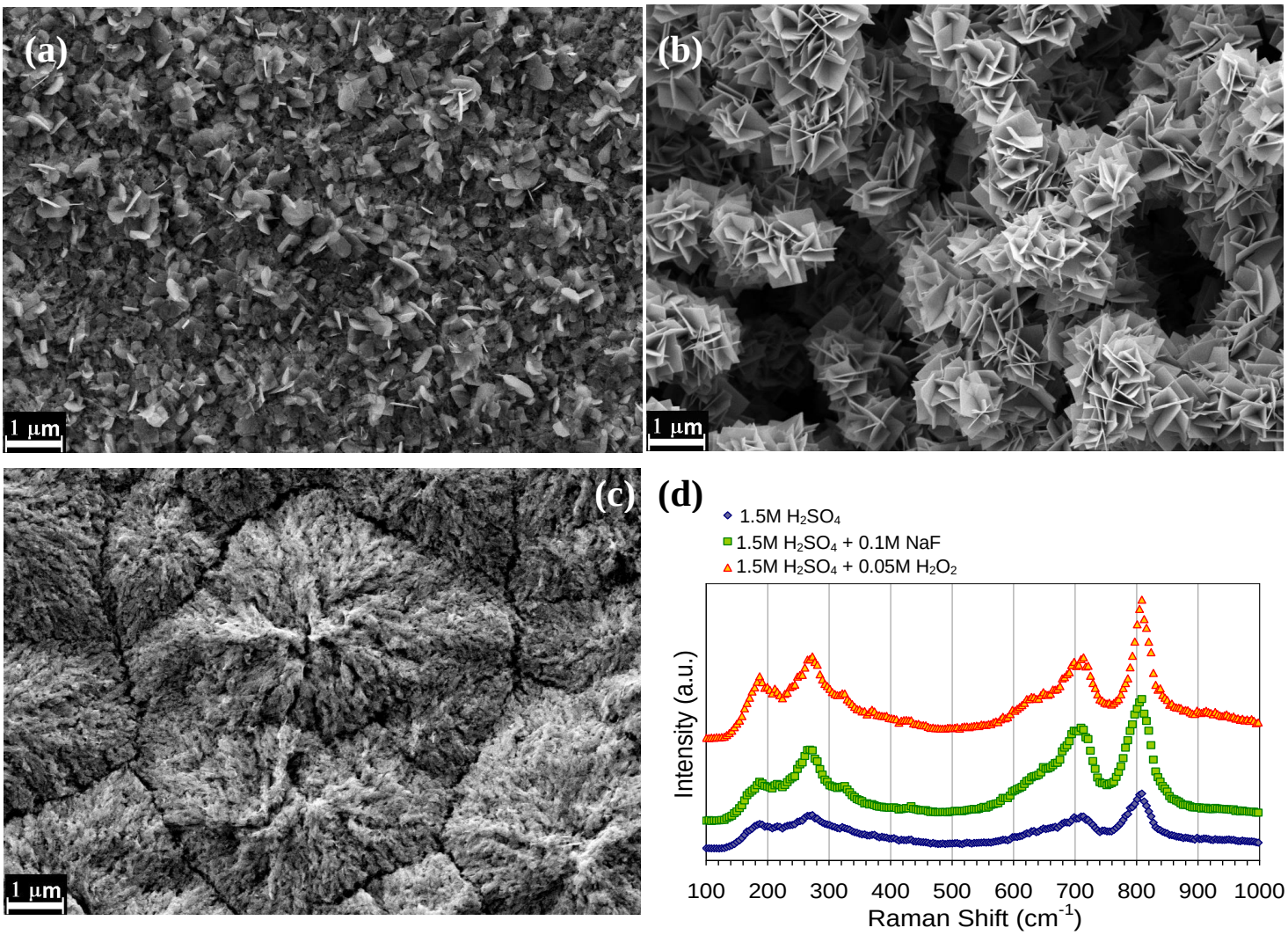
(a)
1 µm
(b)
1 µm
(c)
1 µm
(d)
1.5M H2SO4
1.5M H2SO4 + 0.1M NaF
1.5M H2SO4 + 0.05M H2O2
Intensity (a.u.)
100 200 300 400 500 600 700 800 900 1000
Raman Shift (cm-1)

Figure 2

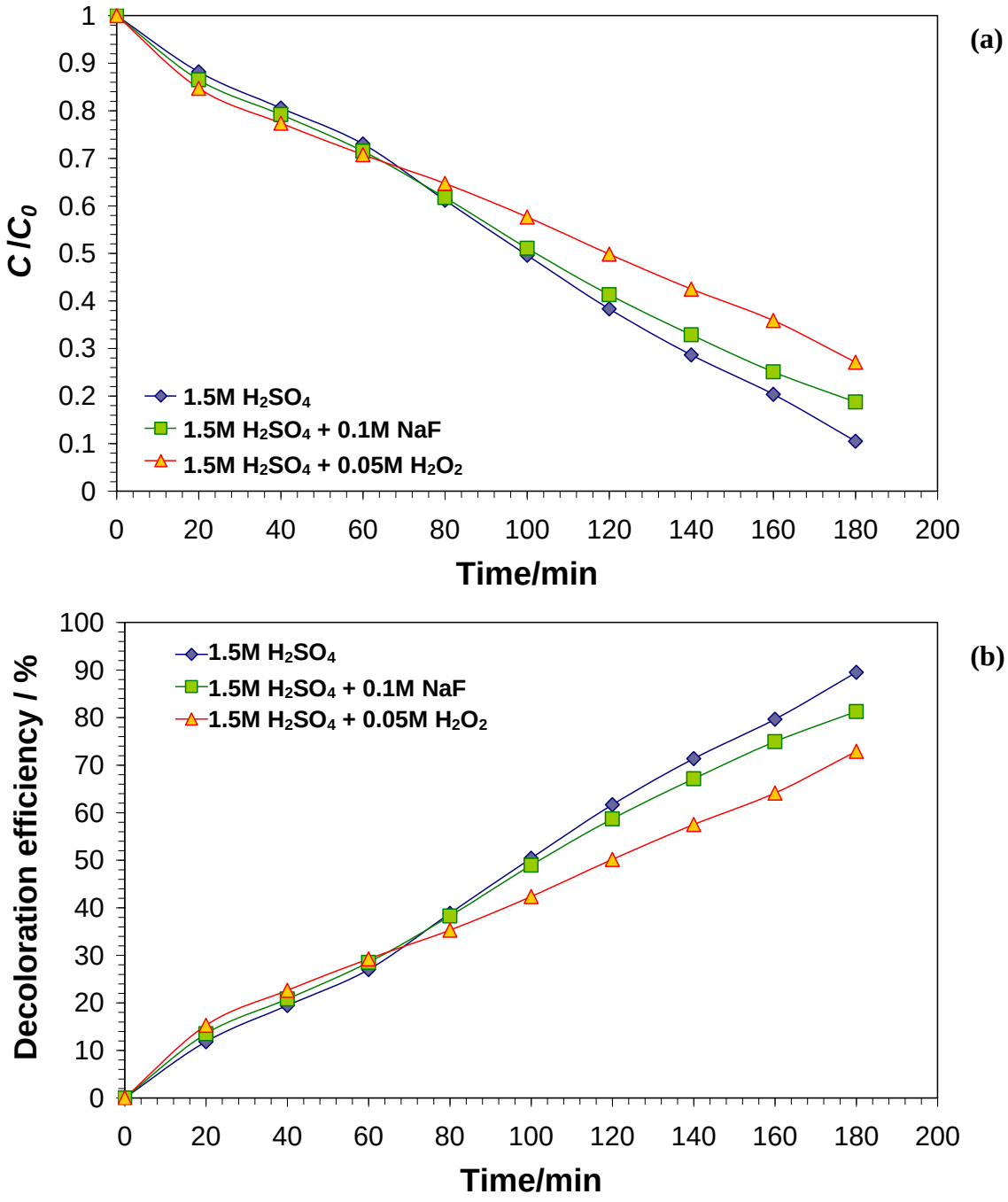
(a)
C /C0
Time/min
1.5M H2SO4
1.5M H2SO4 + 0.1M NaF
1.5M H2SO4 + 0.05M H2O2
(b)
Decoloration efficiency / %
Time/min
1.5M H2SO4
1.5M H2SO4 + 0.1M NaF
1.5M H2SO4 + 0.05M H2O2

Figure 3

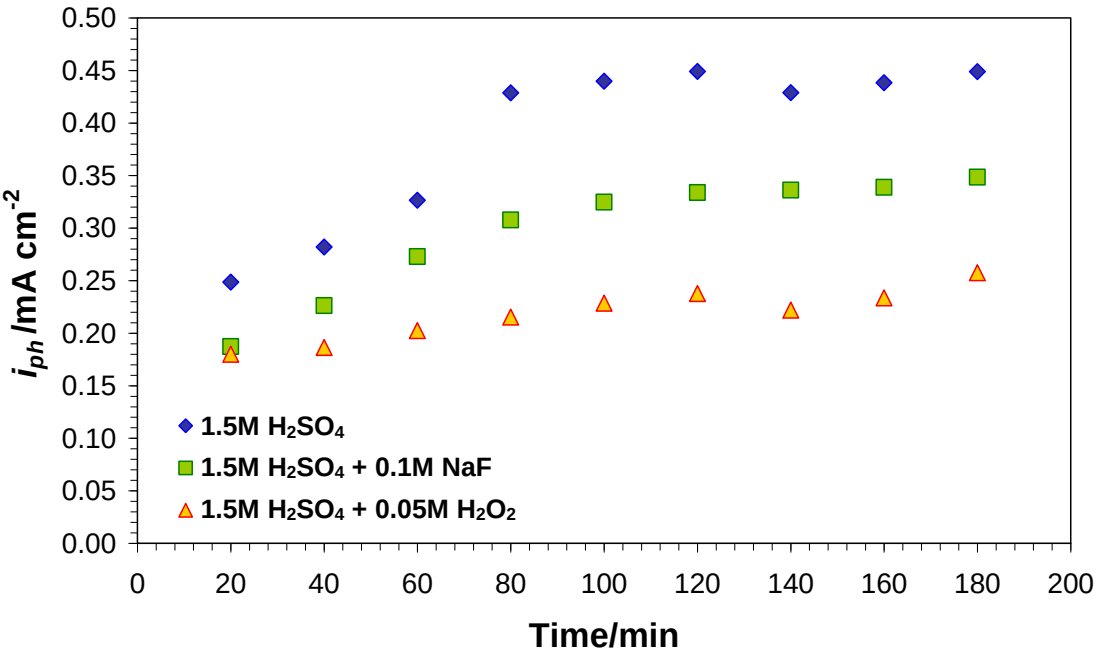
0.50
0.45
0.40
0.35
0.30
0.25
0.20
0.15
0.10
0.05
0.00
i_{ph}/mA cm^{-2}
0
20
40
60
80
100
120
140
160
180
200
Time/min
1.5M H_2SO_4
1.5M H_2SO_4 + 0.1M NaF
1.5M H_2SO_4 + 0.05M H_2O_2

Figure 4

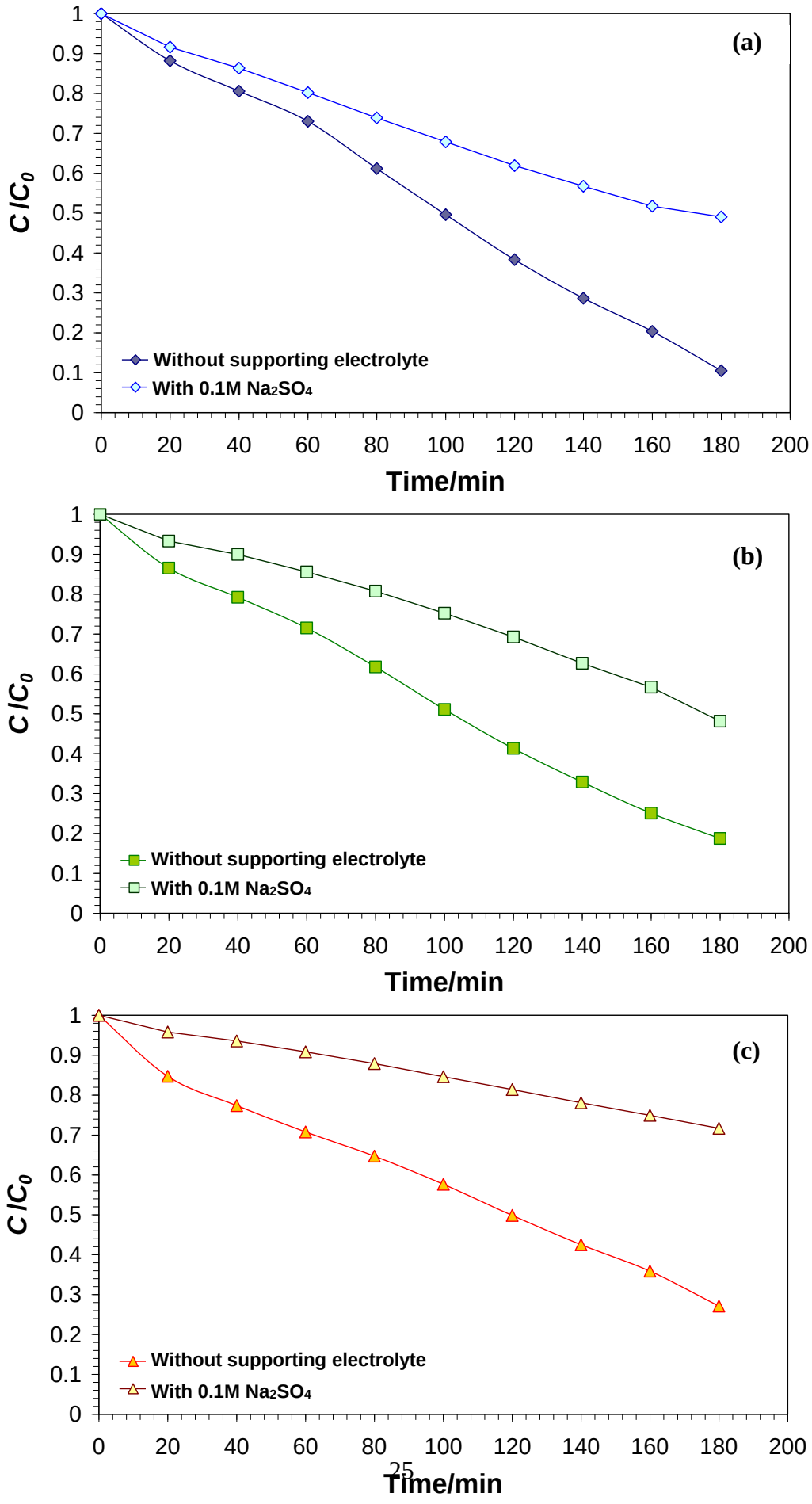
(a)
C /C0
Time/min
Without supporting electrolyte
With 0.1M Na2SO4
(b)
C /C0
Time/min
Without supporting electrolyte
With 0.1M Na2SO4
(c)
C /C0
Time/min
Without supporting electrolyte
With 0.1M Na2SO4

Figure 5

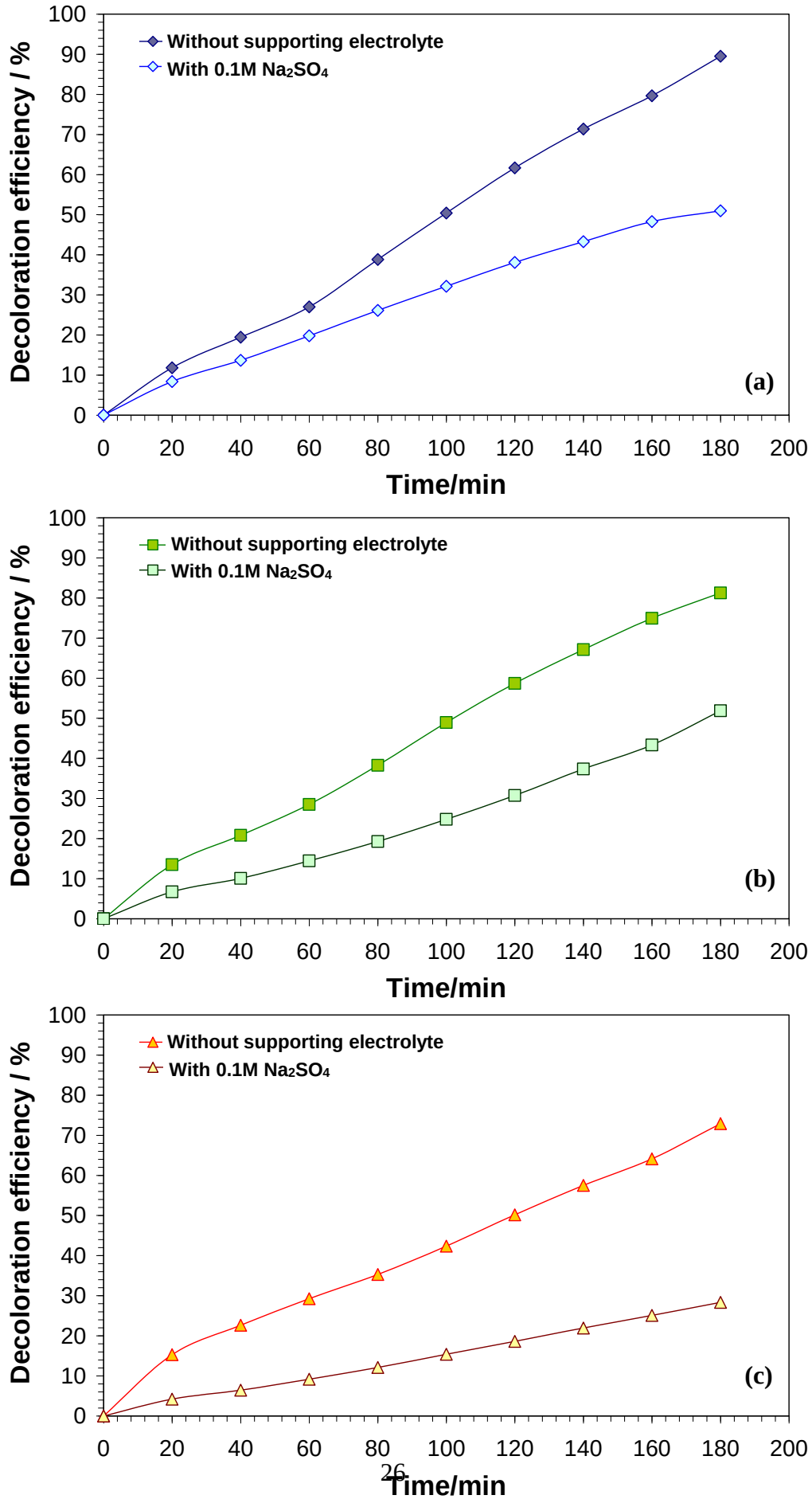
Without supporting electrolyte
With 0.1M Na2SO4
Decoloration efficiency / %
Time/min
(a)
(b)
(c)

Figure 6

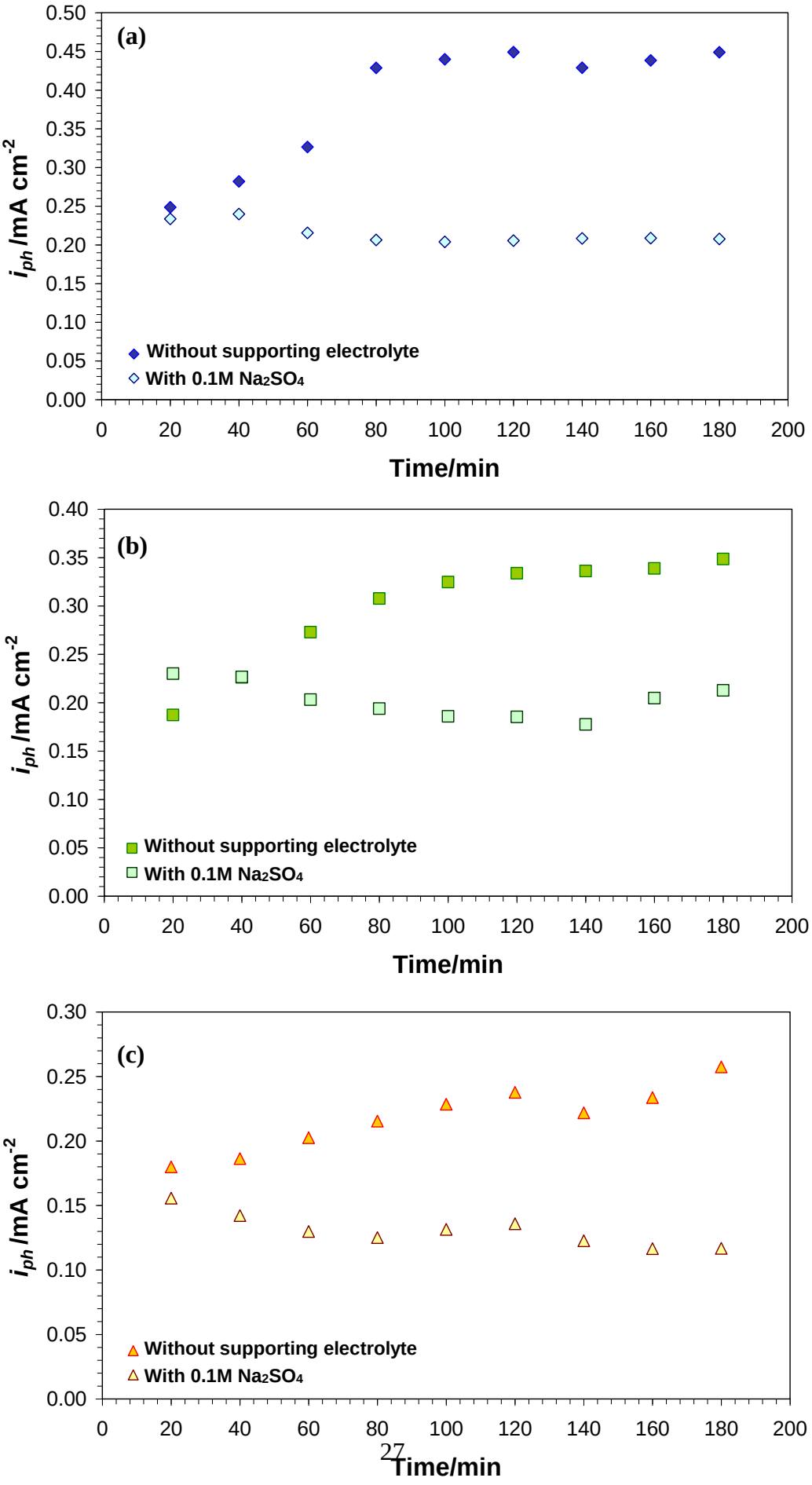
(a)
i_{ph} /mA cm^{-2}
Time/min
Without supporting electrolyte
With 0.1M Na_2SO_4
(b)
i_{ph} /mA cm^{-2}
Time/min
Without supporting electrolyte
With 0.1M Na_2SO_4
(c)
i_{ph} /mA cm^{-2}
Time/min
Without supporting electrolyte
With 0.1M Na_2SO_4

Figure 7

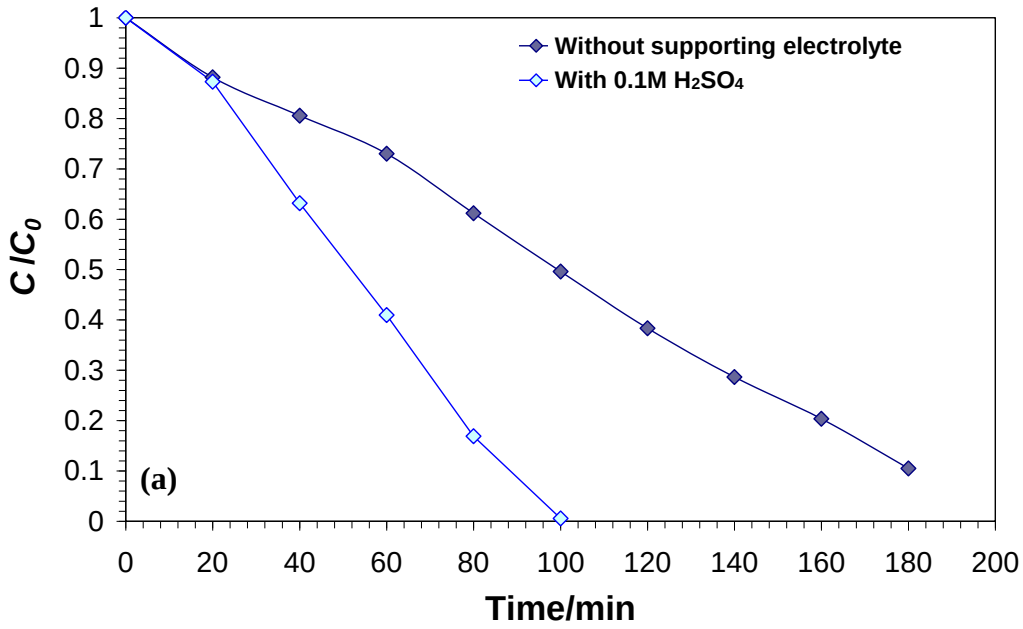
Without supporting electrolyte
With 0.1M H2SO4
C /C0
Time/min
(a)

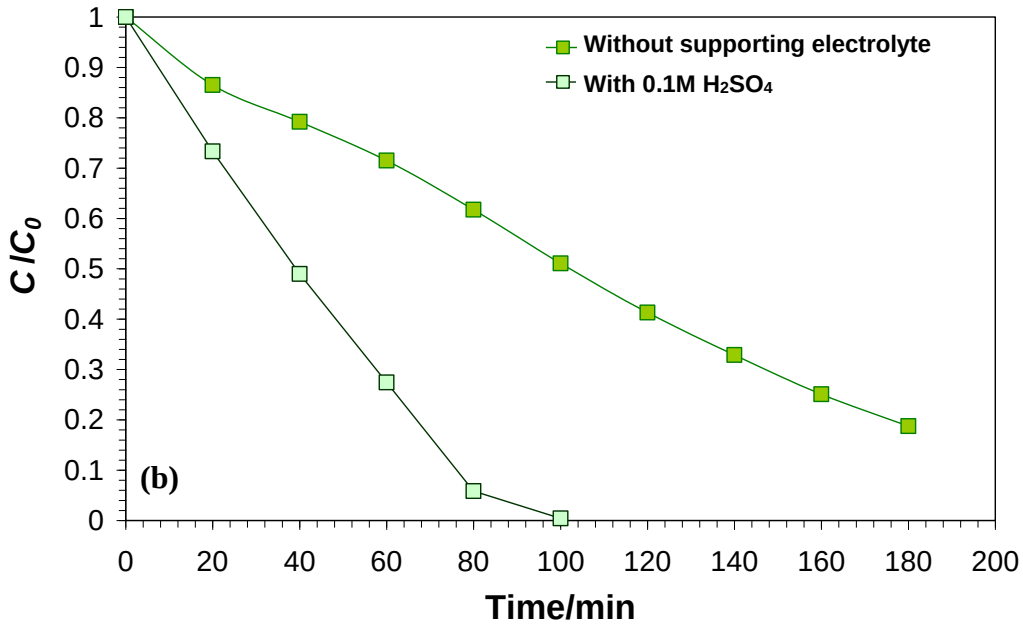
Without supporting electrolyte
With 0.1M H2SO4
C /C0
Time/min
(b)

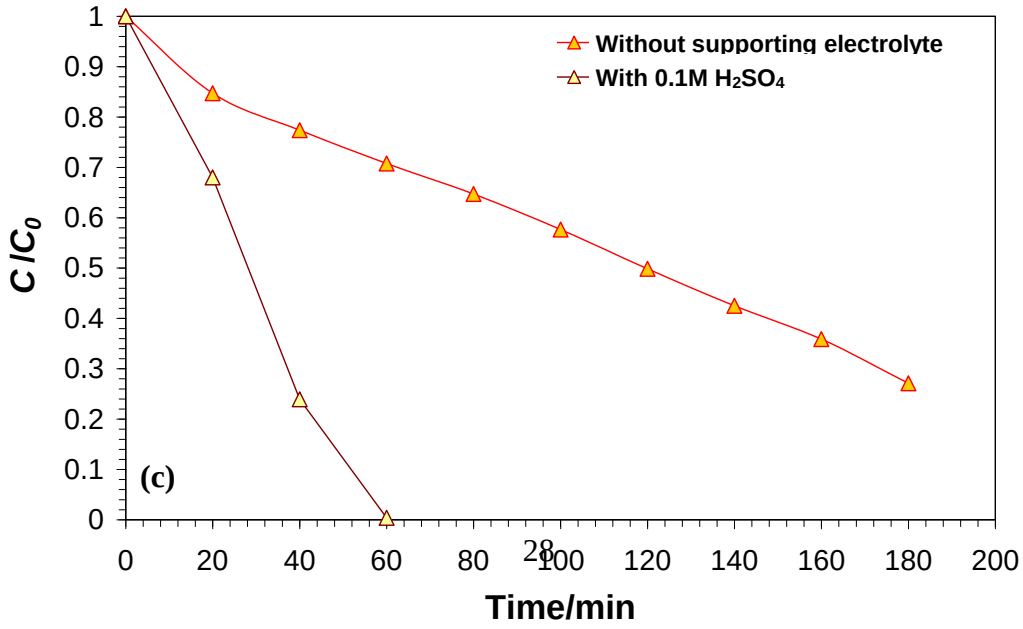
Without supporting electrolyte
With 0.1M H2SO4
C /C0
Time/min
(c)

Figure 8

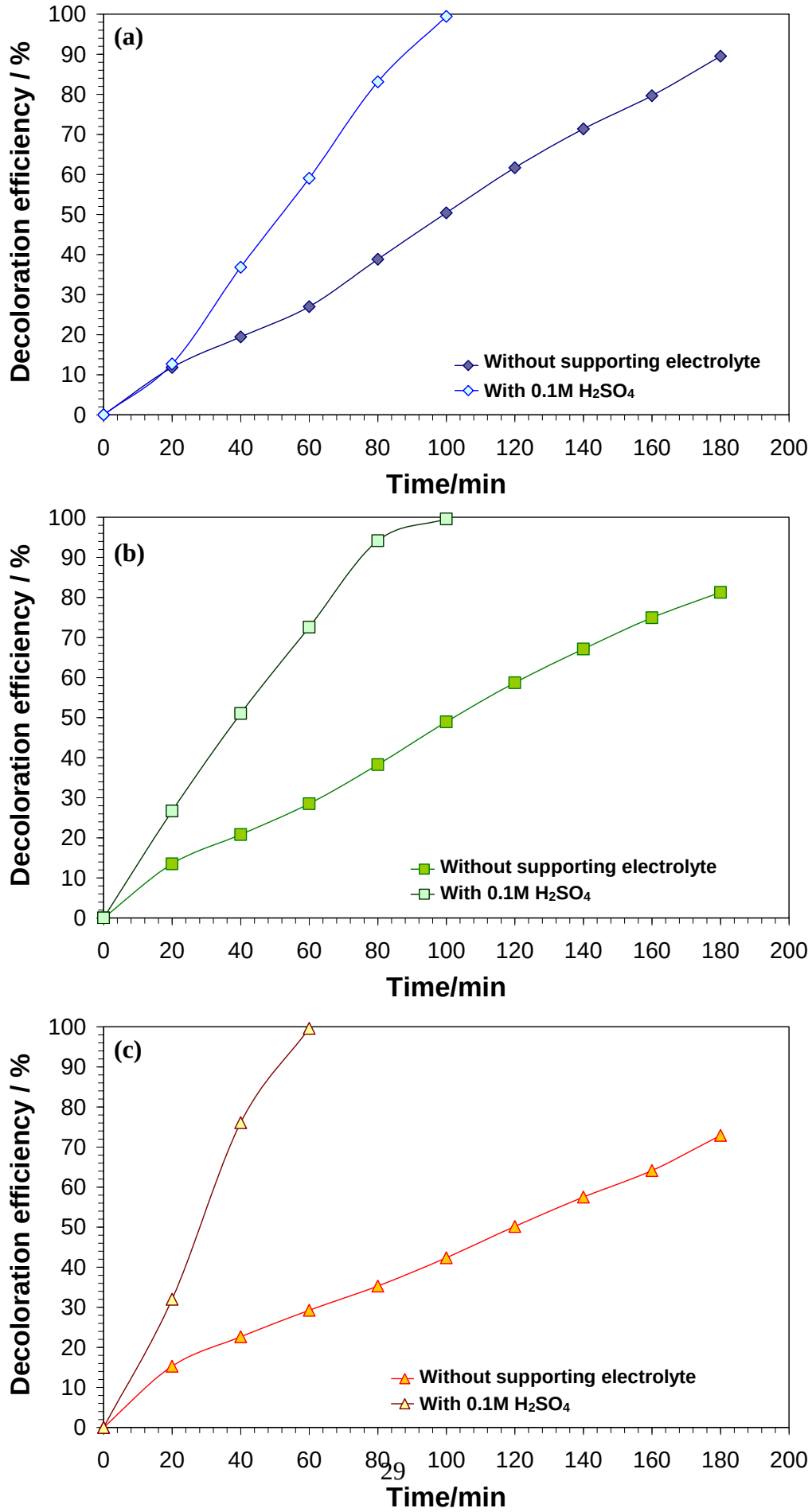
(a)
Decoloration efficiency / %
Time/min
Without supporting electrolyte
With 0.1M H2SO4
(b)
Decoloration efficiency / %
Time/min
Without supporting electrolyte
With 0.1M H2SO4
(c)
Decoloration efficiency / %
Time/min
Without supporting electrolyte
With 0.1M H2SO4

Figure 9

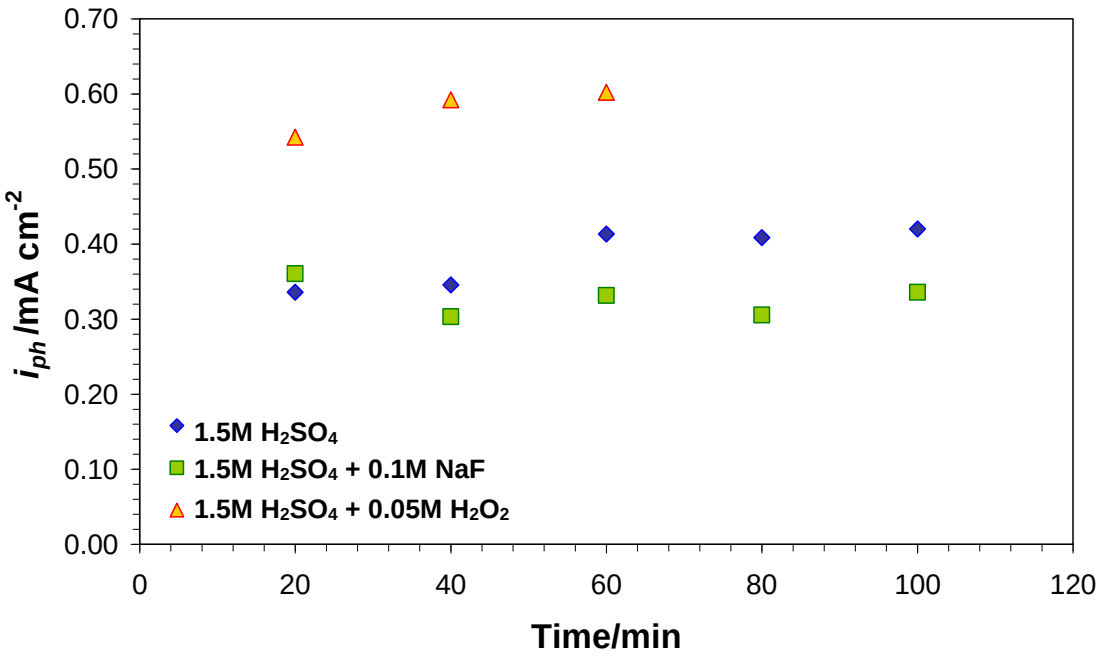

Figure 10